

Tradeoffs Between Wireless Communication and Computation in Closed-loop Implantable Devices

M. Tariqus Salam^{1,2}, Hossein Kassiri¹, Nima Soltani¹, Haoyu He¹,
Jose Luis Perez Velazquez², Roman Genov¹

¹ Department of Electrical and Computer Engineering, University of Toronto, Canada; Email: tariq@eecg.utoronto.ca
² Brain and Behavior Programme and Division of Neurology, Hospital for Sick Children, University of Toronto, Canada

Abstract—This paper discusses general tradeoffs between wireless communication and computation in closed-loop implantable medical devices for neurological applications. Closed-loop devices enable neural monitoring, automated diagnostics and treatment of neurological disorders. Several topologies for the loop are discussed, including within the implant, as well as implemented with a wearable, handheld or stationary processor. Common wireless communication data rate and range requirements and algorithmic computational requirements are summarized. As a case study, a 0.13 μm CMOS neurostimulator SoC for closed-loop treatment of intractable epilepsy is presented. Its triple-band radio with a 1m 230Mbps pulse-radio, a 2m 46Mbps pulse-radio 2, and a 10m 1.2Mbps FSK radio provides a versatile transcutaneous interface. The in-implant processor has constrained computational resources which results in a limited detection performance - seizure detection sensitivity of 87%. A higher-performance signal processing algorithm implemented on a stationary device within a loop enhances the seizure detection performance which was improved to a sensitivity of 98% with three times fewer false alarms. This comes at the cost of an increased wireless transmitter power budget, if communicated directly. These results illustrate a fundamental tradeoff between the communication and computation in closed-loop electronic therapies for neurological disorders.

I. INTRODUCTION

Neurological disorders are estimated to affect as many as a billion people worldwide. Conventional diagnostic systems (e.g., MRI) provide confined temporal information about a neurological condition. Traditional pharmaceutical treatments often have limited overall therapy efficacy [1]. Drug resistance and drug related side-effects are commonly observed. Thus, a large diagnostics and treatment gap is currently present in the modern health care system. A promising approach for reducing the burden of neurological disorders is a comprehensive medical device for continuous monitoring of a patient's health status and providing real-time feedback to warn of or prevent a medical emergency.

Continuous patient health monitoring and real-time feedback have already benefited from microtechnology advancement in the fields of wireless communication and signal processing. However, major barriers to long-term use are high-data-rate wireless communication and advanced signal processing in real-time, both on a tight energy budget of an implanted or a body-worn medical device. High wireless communication data rate is needed for high spatiotemporal-resolution brain monitoring in diagnostics [2]. High-performance signal processing enables reliable vital signs identification and incorporating real-time decision support for early and accurate clinical symptom detection. This may relax the communication link data rate if implemented within a medical device. On the other hand, signal processing requires computational resources

and added complexity in the device design, translating into an increased energy demand.

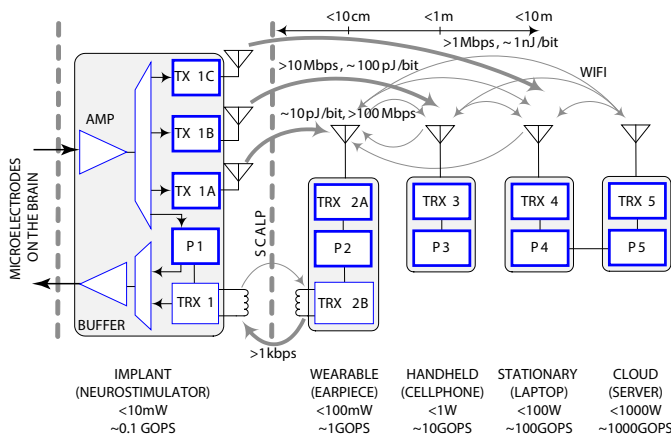
Over the last decade, there has been a growing interest in developing fully-implantable systems-on-chip (SoCs) to perform brain state monitoring, abnormal physiological signal detection and feedback treatment of neurological disorders, such as epilepsy. Such a feedback neurostimulation system with high treatment efficacy requires low-noise compact-channel multi-site neural recording, power-aware signal processing (e.g., on-chip time-advanced seizure detection), versatile wireless diagnostic data communication, and power and configuration telemetry [2], [3].

Ultra-wideband impulse radio (UWB-IR) is often a preferable wireless communication architecture for short-range (<10m) moderate- to high-data-rate (>10Mb/s) transmission [4], [5]. A UWB-IR transmitter (TX) directly radiates a train of short (<1ns) pulses to carry out wide-band data transmission. Compared with the state-of-the-art low-power narrow-band transmitters [6], UWB-IR transmitters offer $\times 10$ or more bandwidth and lower per-bit energy dissipation [4]. In many implants, the battery constitutes the main source of energy, which constrains the implant's functionality and lifetime.

In this paper, trade-offs between communication and computation are described, supported by a case study of a SoC for the treatment of epilepsy. A closed-loop treatment mechanism is demonstrated using on-chip monitoring, signal processing, wireless data communication, and feedback neurostimulation. This fully integrated system was fabricated in a silicon area of 4.85mm x 3.3mm using 0.13 μm CMOS technology. The chip benefits from a quad-core DSP for on-chip seizure detection and three wireless transmitters for data communication over three ranges. Power and feedback commands are delivered through an inductive link. An inductive power transfer technology in the implant enables long-term use of the system without the need for battery replacement or charging of such implantable devices. This inductive link also enables low-rate command communication back to the device to close the loop.

II. CLOSED-LOOP ARCHITECTURE

Fig. 1 illustrates a block diagram of a continuous brain monitoring and real-time feedback system. It includes five main blocks: (i) an implant, (ii) a wearable, (iii) a handheld, and (iv) a stationary device. The implant has five components, the processor (P1), the amplifier (AMP), the neurostimulator (BUFFER), the tri-band radio (TX 1A, TX 1B and TX 1C), and the power and data transceiver (TRX1). The implant records neural signals from multiple electrodes using the



TX: TRANSMITTER, RX: RECEIVER, TRX: TRANCEIVER, P: PROCESSOR, GOPS: GIGA OPERATIONS PER SECOND
 Fig. 1. Block diagram of an implantable closed-loop system and wireless communication interfaces with external processors.

TABLE I
 TRADEOFFS BETWEEN COMMUNICATION AND COMPUTATION

Parameter	Implant	Wearable	Handheld	Stationary
Mobility	✓✓✓✓	✓✓✓	✓✓	×
Latency	✓✓✓✓	✓✓✓	✓✓	✓
Energy efficiency	✓✓✓✓	✓✓✓	✓✓	×
Energy for communication	✓✓✓✓	✓✓✓	✓✓	✓
Algorithm complexity	✓	✓✓	✓✓✓	✓✓✓✓
Algorithm accuracy	✓	✓✓	✓✓✓	✓✓✓✓
Heterogeneity	✓	✓✓	✓✓✓	✓✓✓✓
Adaptivity	✓	✓✓	✓✓✓	✓✓✓✓
Cost	✓	✓✓	✓✓✓	✓✓✓✓
Ease of use	×	✓	✓✓	✓✓✓✓

AMP, processes the signals in real-time in P1, and triggers a neurostimulation through BUFFER upon an abnormal signal pattern detection.

Several other options for closing the loop exist. The acquired signal can be transmitted through the tri-band radio to the wearable, handheld, or stationary devices. The wearable device (e.g., an earpiece) is aligned with the implant and attached to the scalp for short-distance data communication (TRX 2A) and inductive power and feedback commands transfer (TRX 2B). The wearable device is more powerful and thus computationally resourceful than the implant. The implant and the wearable are connected by a high-speed wireless connection. As a result, neural signals can be processed in the wearable in real-time instead of the implant. Second, a more complex and accurate algorithm implementation requires a more advanced signal processor. A handheld (e.g., a cell phone) device can receive neural signals from the implant (directly or through the wearable repeater), process the signals with a more complex algorithm and respond to the implant when needed (e.g., upon an abnormal brain state detection). Finally, a stationary device (e.g., laptop), as an external controller, enables clinicians to interact with the implant through radio frequency transmission as needed for adjusting the algorithm, stimulation parameters, changing operating modes, and storing data. The stationary device enables most computationally expensive signal processing of neural data which can further improve the performance. The wearable device performs the authentication for reprogramming the implant. These and several other possible wireless signal paths are depicted in Fig. 1. Table I shows advantages and disadvantages of the closed-loop device when signal processing occurs within

TABLE II

DETECTION PERFORMANCE OF SEIZURE DETECTION ALGORITHMS

Platform	Method	Reference	Algorithm complexity	Sensitivity (%)	Specificity (%)	Early detection time (sec)
Implant	Phase synchrony	[11]	✓	91	86	5
Wearable	FFT + tree	[12]	✓✓	93	97	11
Handheld	Wavelet + ANN	[8]	✓✓✓	96	89	25
Stationary	Extreme learning	[9]	✓✓✓✓	98	92	34

device or with wearable, handheld or stationary devices.

III. COMPUTATIONAL REQUIREMENTS

Available computational capability versus algorithmic performance is a key tradeoff for an efficient closed-loop implantable device. In the case of epilepsy, the challenges in seizure onset detection are variabilities in signal amplitude, frequency, pattern, and also varying spatiotemporal dynamics of the brain. Thus, a relatively high computational capability is required in signal processing to address all these variabilities and detect a seizure effectively. Many algorithms have been proposed for seizure detection [7]–[9]. These algorithms were carried out offline using a stationary device (e.g., laptop). These types of algorithms cannot be employed in a low-power implantable microchip due to their extensive computational requirements. More recently, lower-complexity seizure detection algorithms with moderate detection performance have been proposed for in-implant integrated seizure detection [2], [3], [10].

In this paper, four different seizure detection algorithms were selected to explore their performance on four different platforms. The first algorithm is for an implant, second for a wearable, third for a handheld and the fourth for a stationary device. The first algorithm is based on phase synchronization between two signals [11]; second is based on Fast Fourier transformation and a decision tree [12]; the third is based on discrete wavelet transform and artificial neural network for the handheld [8]; and the fourth is based on nonlinear features, such as approximate entropy (statistical analysis), hurst exponent (correlation properties), detrended fluctuation analysis (temporal correlations), and also machine learning (extreme learning) [9]. Performances of the four algorithms were evaluated using intracerebral EEG (iEEG) recordings of five patients with epilepsy and are summarized in Table II. The detection performance improves with the increase of the algorithm complexity which requires computational power.

IV. WIRELESS COMMUNICATION

Wireless data transmission rate and range are also critical design criteria for an efficient closed-loop implantable device. The high-rate spatiotemporal information and extensive signal processing are the key parameters for implementation of complex algorithms. A high-rate data connection enables high-performance signal processing algorithms in the wearable, handheld or stationary device as a proxy for the implant. Many RF wireless transmitters have been introduced for low-power moderate-rate and high-rate data transmission applications. Table III includes several transmitters and their features. Short-distance data transmission yields a higher data rate as needed for real-time signal processing in a remote device and low-latency feedback commands.

TABLE III
A COMPARATIVE STUDY ON WIRELESS TRANSMITTERS

Device	Data rate (bps)	Output power (dBm)	Average power (mW)	Modulation	Energy per bit (J/bit)	TX Efficiency (%)	Range (m)
ANT	60k	0	8.7		147n	11.5	30
ZigBee	250 k	0 to -20	14.8	OQPSK	59.4n	6.7	10 - 100
Zarlink	800k	4.5 to -17	16.5	FSK	20.6n	6	3
Nordic RF module	2M	0 to -16	40.5	GFSK	20n	2.5	100
TI RF module	600k	+12 to -30	7.2	FSK	12n	14	30
Low-power bluetooth	3M	+4 to -20	30.7	GFSK	10.2n	3.2	1 - 100
TX 1C	1.2M	-20 to 0	3.7	FSK	3.1n	15	10
TX 1B	46M	-1	3.8	UWB	85p	21	1
TX 1A	230M	-1	3.8	UWB	17p	21	0.1

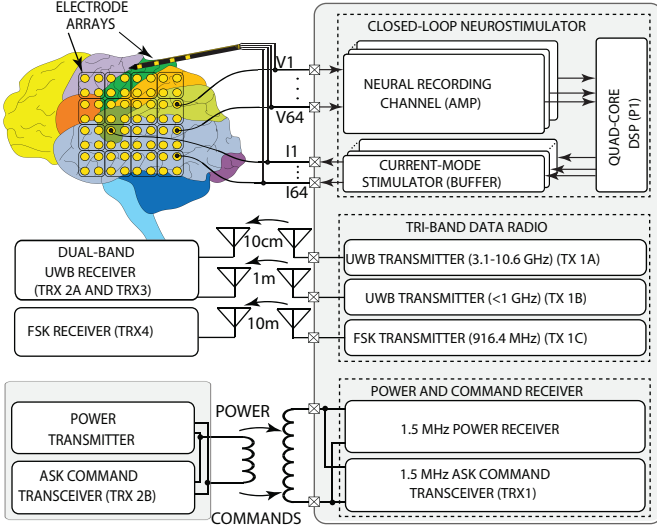


Fig. 2. A simplified functional diagram of the neurostimulator SoC and peripheral blocks.

V. CASE STUDY: SEIZURE-ABORTING NEUROSTIMULATOR

Fig. 2 illustrates the system architecture of a closed-loop neurostimulator SoC presented here as an example. This device includes 64 recording channels, a quad-core low-power DSP, 64 current-mode neurostimulators, a triple-band RF transmitter, and an inductive command and power receiver [13].

A. Triple-Band Radio

A triple-band RF radio is designed to transmit recorded iEEG data transcutaneously to the wearable, handheld, or stationary devices. The 3.1-10.6GHz UWB short-range (10cm) transmitter (TX 1A) communicates through the scalp to a wearable receiver. The under-1GHz UWB mid-range (1m) transmitter (TX 1B) communicates to a handheld receiver. The 915MHz FSK long-range (10m) transmitter (TX 1C) communicates to an indoor stationary receiver. Energy is transmitted by a single coil (TRX 2B) through a multi-coil cellular inductive link at 1.5MHz frequency. The power transmitter outputs 30mW maximum power for the 12cm maximum transmission distance with power efficiency of 40% [13]. An ASK command receiver (RX1) reuses the same inductive link to recover transmitted commands and the clock.

B. On-Chip DSP

An epileptic seizure detection algorithm was introduced in our previous studies [3], [11]. The detection of the seizure

onset was based on the fluctuations in a phase synchrony index (R) between two iEEG recordings. The index R is proportional to the fluctuations in the phase difference of two channels. It is estimated as the absolute value of the derivative of the time series: $|d(\Delta\phi)/dt|$, where $\Delta\phi$ is the phase difference between two selected channels. Generally, R is measured using the mean phase coherence statistic (1 sec running window), which is defined as $R = |\langle e^{d(\Delta\phi)} \rangle|$. The quad-core low-power digital signal processor (DSP) in Fig. 2 is designed to compute the first derivative of the neural signals phase synchrony (i.e., spatial neural synchrony fluctuations), 16 channels per core.

C. Stimulator circuit

Fig. 2 also shows a current-mode stimulator in the feedback path of the closed-loop neurostimulator, which triggers a programmable train of biphasic current stimulation upon a seizure onset detection.

D. Trade-offs

For this design, the experimentally-measured power consumption of the on-chip processor is $897\mu\text{W}$ for a clock frequency of 10MHz and supply voltage of 1.15V. To reduce power consumption, both supply voltage and clock frequency could be reduced to 0.85V and 2.5MHz, respectively, at the cost of a higher detection latency. For a 1.15V supply at 2.5MHz the processor dissipates $231\mu\text{W}$, and for a 0.85V supply at 2.5MHz and 10MHz the processor dissipates $102\mu\text{W}$ and $412\mu\text{W}$, respectively. Also for only one pair of channels, operating at 1.7kS/s the processor dissipates $3.6\mu\text{W}$ when operating with a 0.85V supply.

Based on these power figures, the seizure detector processor dissipates $3.6\mu\text{W}/\text{channel}$ and has an energy efficiency of 210pJ/bit. For processing off-chip this requires an RF wireless transmitter such as the ones listed in Table III. The total power consumption for transmission is 3.7mW and 3.8mW for the FSK and UWB transmitters, respectively. The ASK wireless receiver used to receive stimulation commands (within TRX1) has a power consumption of $350\mu\text{W}$. Overall, this yields an energy efficiency of 3.37nJ/bit for the FSK TX 1C (10m range), 90pJ/bit for the UWB TX 1B (1m range), and 18pJ/bit for the UWB TX 1A (10cm range).

Based on the above, achieving the 98% detection sensitivity while communicating by means of the FSK TX directly to a stationary processor comes at the cost of degrading energy efficiency by a factor of 16. Communicating to a hand-held processor using a medium-range high-data-rate UWB TX yields $2.3\times$ better energy efficiency and 5% higher sensitivity, as compared to an implanted signal processor, at the cost of 20s higher latency. Finally, communicating to a wearable processor using a short-range medium-data-rate UWB TX yields $11.6\times$ better energy efficiency and 2% higher sensitivity at the cost of 6s longer latency. Depending on how: (a) energy efficiency of detection, (b) latency, and (c) accuracy are prioritized, one of the four options described can be used. A solution acceptable for most cases is to use a wearable data repeater, assuming the cost and the ease of use are tolerable.

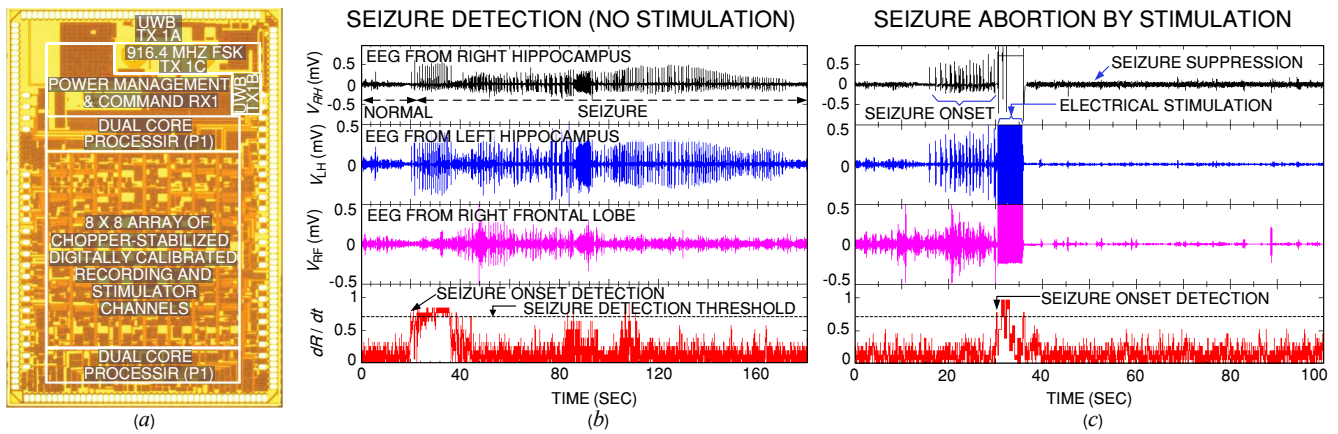


Fig. 3. (a) Micrograph of the 16mm^2 closed-loop neurostimulator and in-vivo experiment results example: (b) real-time seizure detection and (c) closed-loop seizure suppression.

E. In vivo experiment

The closed-loop neurostimulator was implemented in a $4.85\text{mm} \times 3.3\text{mm}$ SoC using a standard $1\text{P}8\text{M}$ $0.13\mu\text{m}$ CMOS technology. Micrograph of the chip is shown in Fig. 3. The integration area was reduced by 80% compared with an equivalent AC-coupled implementation [3]. The SoC was validated in a chronic experiment using a rodent model of epilepsy. Four Wistar rats were intraperitoneally injected with kainic acid which induced recurrent spontaneous motor seizures within one to two months. The rats underwent craniotomy for both hippocampi and frontal lobe microelectrodes implantation. The rats were divided into two equal groups: the non-stimulation group and the stimulation group. In each rat, the electrodes were connected to the presented SoC for automatic seizure detection. Each rat was also video monitored for seizure labeling. Fig. 3 (b) shows an example of in-vivo real-time seizure detection in the non-stimulation group.

In the stimulation group the SoC was also configured to trigger the closed-loop electrical stimulation in response to a seizure onset detection. Fig. 3 (c) illustrates the SoC-triggered stimulation upon a seizure onset detection in the stimulation group and the seizure having been suppressed.

The average sensitivity and specificity of the detection were 87% and 95%, respectively. Seizure frequency has been reduced on average by over 76% in the stimulation group compared to the non-stimulation group.

In a second implementation, a four times more complex signal processing algorithm was deployed on a stationary device. This requires a 200kbps wireless data communication forwardlink. As a result, the detection performance was improved to a sensitivity of 98% with three times fewer false alarms. This requires an additional 3.7mW of power within the implant.

VI. CONCLUSION

The closed-loop treatment efficacy is likely to depend on accurate physiological symptom detection. A high-performance signal processing algorithm for multi-site spatiotemporal physiological recording enables early and accurate symptom detection. Often the low-power implant is unable to implement the complex signal processing. The presented implantable SoC benefits from a triple-band wireless transmitter for versatile transcutaneous interfacing. The triple-band radio yields a number of degrees of freedom in wireless communication trading

between energy efficiency of computation and communication.

REFERENCES

- [1] D. K. Nguyen, et al., "The Treatment of Epilepsy: Invasive EEG in presurgical evaluation of epilepsy, Third Edition (eds S. Shorvon, E. Perucca and J. Engel)," *Wiley-Blackwell*, 2009.
- [2] W.-M. Chen, et al., "A fully integrated 8-channel closed-loop neural-prosthetic SoC for real-time epileptic seizure control," *ISSCC* 2013, pp. 286–287.
- [3] K. Abdelhalim, et al. "64-channel UWB wireless neural vector analyzer SOC with a closed-loop phase synchrony-triggered neurostimulator," *JSSC* vol. 48, no. 10, pp. 2494–2510, 2013.
- [4] P. Mercier, D. Daly, and A. Chandrakasan, "An energy-efficient all digital UWB transmitter employing dual capacitively-coupled pulse-shaping drivers," *IEEE J. Solid-State Cir.*, vol. 44, no. 6, pp. 1679–1688, Jun. 2009.
- [5] F. Padovan, A. Bevilacqua, and A. Neviani, "A 20Mb/s, 2.76 pJ/b UWB impulse radio TX with 11.7% efficiency in 130 nm CMOS," *ESSCIRC*, 287–290, Sep. 2014.
- [6] Liu, Yao-Hong, et al. "A 3.7 mW-RX 4.4 mW-TX fully integrated Bluetooth Low-Energy/IEEE802. 15.4/proprietary SoC with an ADPLL-based fast frequency offset compensation in 40nm CMOS," *ISSCC*, pp. 236–237, Feb. 2015.
- [7] G. Sukhi, and G. Jean, "An automatic warning system for epileptic seizures recorded on intracerebral EEGs," *Clinical neurophysiology*, vol. 116, pp. 2460–2472, 2005.
- [8] L. Guo et al., "Automatic epileptic seizure detection in EEGs based on line length feature and artificial neural networks," *Journal of Neuroscience Methods*, vol. 191-1, pp. 101–9, 2010.
- [9] Q. Yuan et al., "Epileptic EEG classification based on extreme learning machine and nonlinear features," *Epilepsy Res.*, vol. 96, no. 1, pp. 29–38, 2011.
- [10] N. Verma et al., "A micro-Power EEG acquisition SoC with integrated feature extraction processor for a chronic seizure detection system," *IEEE JSSC*, vol. 45, no. 4, pp. 804–16, 2010.
- [11] J. L. Perez Velazquez et al., "Experimental observation of increased fluctuations in an order parameter before epochs of extended brain synchronization," *J. Biol. Phys.*, vol. 37, pp. 141–152, 2011.
- [12] K. Polat and S. Gne, "Classification of epileptiform EEG using a hybrid system based on detection tree classifier and fast Fourier transform," *Applied Mathematics and Computation*, vol. 186, no. 2, pp. 1017–1026, 2007.
- [13] H. Kassiri et al., "Inductively-Powered Direct-Coupled 64-Channel Chopper-Stabilized Epilepsy-Responsive Neurostimulator with Digital Offset Cancellation and Tri-Band Radio," *IEEE ESSCIRC*, pp. 95–98, 2014.
- [14] N. Soltani et al., "0.13 μm CMOS 230Mbps 21pJ/b UWB-IR transmitter with 21.3% efficiency," *IEEE ESSCIRC*, pp. 352–355, 2015.